

# Jitter Does Matter: Adapting Gaze Estimation to New Domains

Ruicong Liu<sup>1</sup> Yiwei Bao<sup>1</sup> Mingjie Xu<sup>1</sup> Haofei Wang<sup>2</sup> Yunfei Liu<sup>1</sup> Feng Lu<sup>1,2,\*</sup>

<sup>1</sup> State Key Laboratory of VR Technology and Systems, School of CSE, Beihang University

<sup>2</sup> Peng Cheng Laboratory, Shenzhen, China

{liuruicong, baoyiwei, xumingjie, lyunfei, lufeng}@buaa.edu.cn wanghf@pcl.ac.cn

## Abstract

Deep neural networks have demonstrated superior performance on appearance-based gaze estimation tasks. However, due to variations in person, illuminations, and background, performance degrades dramatically when applying the model to a new domain. In this paper, we discover an interesting gaze jitter phenomenon in cross-domain gaze estimation, *i.e.*, the gaze predictions of two similar images can be severely deviated in target domain. This is closely related to cross-domain gaze estimation tasks, but surprisingly, it has not been noticed yet previously. Therefore, we innovatively propose to utilize the gaze jitter to analyze and optimize the gaze domain adaptation task. We find that the high-frequency component (HFC) is an important factor that leads to jitter. Based on this discovery, we add high-frequency components to input images using the adversarial attack and employ contrastive learning to encourage the model to obtain similar representations between original and perturbed data, which reduces the impacts of HFC. We evaluate the proposed method on four cross-domain gaze estimation tasks, and experimental results demonstrate that it significantly reduces the gaze jitter and improves the gaze estimation performance in target domains.

## 1 Introduction

Gaze indicates the direction along which a person is looking. It has been adopted in various applications, such as semi-autonomous driving (Demiris 2007; Majaranta and Bulling 2014; Park, Jain, and Sheikh 2013) and human-robot interaction (Admoni and Scassellati 2017; Terzioğlu, Mutlu, and Şahin 2020; Wang et al. 2015). With an increasing demand for predicting user intent implicitly, appearance-based gaze estimation has attracted more attention recently. To train the gaze estimator using deep learning neural networks, a number of large-scale datasets have been proposed (Zhang et al. 2020, 2017; Funes Mora, Monay, and Odobez 2014; Kellnhofer et al. 2019).

However, due to variations in subjects, backgrounds, and illuminations, the performance of deep learning-based gaze estimation algorithms deteriorate significantly when applying the model trained in one dataset to new datasets. Recently, several techniques have been applied to address this cross-domain problem, such as adversarial learning (Tzeng et al. 2017; Cui et al. 2020), few-shot learning (Park et al.

2019; Yu, Liu, and Odobez 2019) and self-training (Cai, Lu, and Sato 2020). Among them, unsupervised domain adaptation (UDA) method (Wang et al. 2019; Kellnhofer et al. 2019; Liu et al. 2021c) is one of the promising approaches that attracts much attention. While requiring no labels makes it more applicable to real-world scenarios, it also makes the task more challenging.

Existing approaches usually optimize the gaze accuracy during adaptation directly. Instead, we design an approach that starts with the analysis of a phenomena we observed that occurs in crossing domain tests. Where we can look for the factors that cause the problems, and the factors can then be used as guidance for us to find a more explainable solution for domain adaptation.

In this paper, we observe the gaze jitter phenomena: two very similar images could be predicted with gazes severely deviated (shown in Fig. 1), particularly when crossing domains. As shown in Fig. 1, on the test set in the source domain, the model gives similar predictions when the input images are similar. In contrary, in the target domain, even if the input images are very similar, the model may still give predictions that are severely deviated. In this paper, we name this phenomenon as gaze jitter, and in addition, we consider gaze jitter as a manifestation of gaze error across domains, and use this phenomenon as a starting point to find a solution for domain adaptation.

Based on the above observation, we start to analyze why the gaze jitter phenomenon occurs and discover an important factor, *i.e.*, the high-frequency component (HFC), which introduces gaze jitter problem and lowers the gaze estimation accuracy. Inspired by this, we propose our gaze adaptation framework. At first, our framework adds additive HFC to the input data, then it employs contrastive learning to keep the consistency between the original data and the perturbed data, thus making the model learn features with less impact of high-frequency component. Our method leads to significant jitter reduction and performance improvement on various cross-domain gaze estimation tasks. The primary contributions of this paper are summarized as follows:

- For the first time, we discover the gaze jitter problem on cross-domain gaze estimation tasks. We find that high-frequency component is an important factor introducing jitters.
- We propose a framework for cross-domain gaze estima-

\*Corresponding Author.

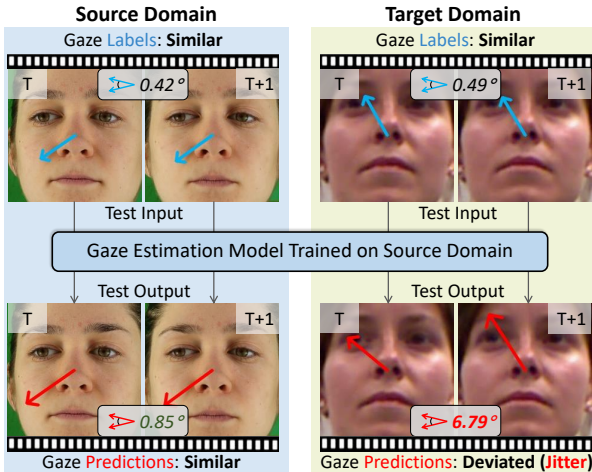


Figure 1: We observe **gaze jitter** during cross-domain gaze estimation. Even though similar input images are expected to output close gaze directions, the predicted output can be severely deviated in target domain (bottom-right). We find such a gaze jitter a good indicator to help analyze and optimize cross domain gaze estimation.

tion that suppresses the influence of high-frequency component, resulting in less jitter and better cross-domain gaze estimation accuracy.

- Experimental results demonstrate that our method exhibits exceptional performances on four gaze domain adaptation tasks using only a small number of target images.

## 2 Related Work

### 2.1 Appearance-based gaze estimation

Appearance-based gaze estimation aims to predict the human gaze from appearance. Zhang *et al.* proposed the first CNN-based gaze estimation method (Zhang *et al.* 2017), which uses eye images. With the release of many large-scale gaze datasets (Zhang *et al.* 2020; Funes Mora, Monay, and Odobez 2014; Kellnhofer *et al.* 2019; Zhang *et al.* 2017), appearance-based gaze estimation has attracted more and more attention. Many methods have been proposed to estimate accurate gazes on public datasets. (Cheng *et al.* 2020; Guo *et al.* 2020; Shrivastava *et al.* 2017; Wang *et al.* 2019).

However, most studies focus on the gaze estimation within a single dataset (Lu *et al.* 2014; Park *et al.* 2019; Yu, Liu, and Odobez 2019). Due to the diversity of different datasets, almost all gaze estimation methods suffer from poor cross-domain capability (Cheng *et al.* 2020; Wang *et al.* 2019). Recent works (Liu *et al.* 2021c; Zhang *et al.* 2020) investigated the cross-domain capability of a gaze estimator, which improves the applicability to real-world scenes.

### 2.2 Unsupervised domain adaption

Unsupervised domain adaption (UDA) is a transfer learning task that requires no target labels. Previous UDA approaches can be divided into three categories: discrepancy, reconstruction, and adversarial methods. Discrepancy methods

aim to minimize the domain gap using some distance metrics, such as Maximum Mean Discrepancy (MMD) (Ghifary, Kleijn, and Zhang 2014) and Local Maximum Mean Discrepancy (LMMD) (Zhu *et al.* 2020). Reconstruction methods (Glorot, Bordes, and Bengio 2011; Bousmalis *et al.* 2016) use a reconstruction strategy that allows a model to learn features from both domains (Wang and Deng 2018). Adversarial methods are inspired by the generative adversarial network (GAN) (Goodfellow *et al.* 2014). In (Ganin and Lempitsky 2015; Tzeng *et al.* 2017; Cui *et al.* 2020; Yu *et al.* 2019), they make a domain discriminator and a generator play a min-max game, thereby explicitly reducing the distance between the source and target domains.

However, most existing UDA methods have been designed for classification or semantic segmentation tasks. Gaze estimation is a typical regression task, its continuous label space makes it even more challenging.

### 2.3 Adversarial attack

The goal of the adversarial attack is to generate adversarial noise. Although this noise is a type of high-frequency component that usually cannot affect human cognition, recent studies (Goodfellow, Shlens, and Szegedy 2014; Szegedy *et al.* 2013) have shown that deep neural networks are highly vulnerable to it. Although some adversarial attack methods have been proposed (Moosavi-Dezfooli, Fawzi, and Frossard 2016; Su, Vargas, and Sakurai 2019) in the past few years, they mainly follow two ideas proposed by (Goodfellow, Shlens, and Szegedy 2014) and (Madry *et al.* 2017a). Recently, the adversarial attack has been applied to UDA tasks in various fields (Ma *et al.* 2021; Yang *et al.* 2021; Madry *et al.* 2017b; Liu *et al.* 2021a), which reminds us of the potential of applying it to the field of gaze estimation.

### 2.4 Contrastive learning

On UDA tasks, contrastive learning is usually used to help the model learn better representations. It encourages augmentations of the same input to have more similar representations compared to augmentations of different inputs. Common contrastive learning frameworks achieve this aim by constructing two kinds of pairs: positive pairs containing similar instances and negative pairs containing different instances. Then it maximizes the consistency over the positive pairs and pushes apart samples from the negative pairs. Recent contrastive learning studies, *e.g.*, Memory Bank (Wu *et al.* 2018), MoCo (He *et al.* 2020), SimCLR (Chen *et al.* 2020), and PCL (Li *et al.* 2020) have reached considerable improvement on some downstream tasks.

Contrastive learning has been used for UDA in some tasks, such as action recognition (Kang *et al.* 2020) and semantic segmentation (Liu *et al.* 2021b). The significant effect shows the capability of contrastive learning to learn useful representations.

## 3 Motivation

In this section, we observe that gaze jitter is a significant phenomenon in cross-domain gaze estimation. Then, we discover one important factor introducing jitter: high-frequency

component. Finally, we design a framework to adapt the gaze estimation to new domains with the guidance of this discovery.

### 3.1 Gaze Jitter: an Observation in Cross-Domain Gaze Estimation

As we know, the performance of pre-trained gaze estimation model usually degrades in unseen target domains. Most previous works study this problem only focusing the rise of gaze estimation error in target domains. However, along with the rise in error, we observe the gaze jitter phenomenon, *i.e.*, images with similar appearances and labels can be predicted with severely deviated gaze directions. In our further analysis, we find the jitter is significantly larger in the target domain than in the source domain (Fig. 1). To numerically measure the magnitude of jitter, we define a new metric *mean-angular-deviation* (*mav*) as follow.

*Definition.* We denote the test dataset as  $\mathcal{D} = \{(x_i, y_i)_{i=1}^{N_{\mathcal{D}}}\}$ , where  $x_i$  and  $y_i$  denote the  $i$ -th image and the corresponding gaze direction,  $N_{\mathcal{D}}$  is the number of images.  $\{\hat{y}_i\}_{i=1}^{N_{\mathcal{D}}}$  is the prediction from an estimation model. We design *mav* to measure the magnitude of jitter:

$$mav(\mathcal{D}) = \frac{1}{N} \sum_{x_i, x_j \in \mathcal{D}} |\langle \hat{y}_i, \hat{y}_j \rangle - \langle y_i, y_j \rangle|, \quad (1)$$

*s.t.*  $SSIM(x_i, x_j) > \alpha, \langle y_i, y_j \rangle < \beta.$

where  $\langle y_i, y_j \rangle$  indicates the angle between  $y_i$  and  $y_j$ ,  $N$  is the number of image pairs that satisfy the constraint, and *SSIM* measures the similarity between images (Wang et al. 2004). The *mav* calculates the deviation between the angles of the predictions and labels from image pairs with similar appearance and labels. Empirically, we set  $\alpha = 0.75$  and  $\beta = 1^\circ$ .

To briefly verify the correctness of *mav*, we add random noise (Gaussian) with gradually increasing level to the test data, the change of *mav* is illustrated in Fig. 2(a). The *mav* reflects the trend of magnitude correctly, *i.e.*, stronger noise results in stronger jitter.

Using the *mav*, we measure the magnitude of jitter on both source and target domains. Results are shown in Fig. 2(b), and the gaze jitter is indeed more significant on the target domain. Therefore, we treat gaze jitter as a good indicator to help analyze and optimize cross-domain gaze estimation.

### 3.2 Why Does Gaze Jitter Occur?

The question that arises is: *Why does gaze jitter occur?* According to (Wang et al. 2020), CNNs may capture high-frequency component (HFC) that are misaligned with human visual preference. This conclusion is coincide with the observed gaze jitter: images which are similar to human (similar appearance) could be very different to CNN (severely deviated gaze predictions). Therefore, we speculate HFC could also be a factor introducing jitter.

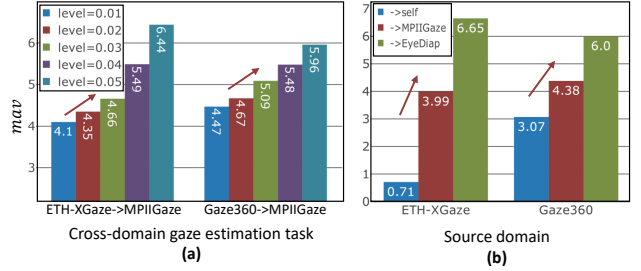


Figure 2: (a) The magnitude of jitter measured by *mav* when adding random noise (Gaussian) with gradually increasing scale to the test data. (b) The magnitude of jitter on the source and target domains. The ETH-XGaze and Gaze360 datasets are employed as source domains, and the MPIIGaze and EyeDiap datasets are used as target domains.

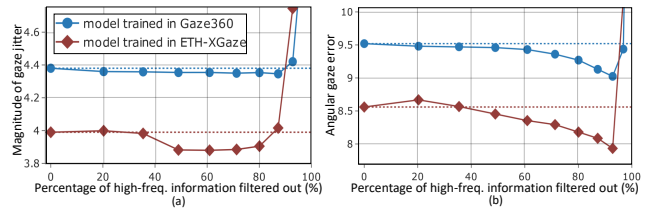


Figure 3: (a) and (b) illustrate the level of gaze jitter and angular gaze error on the target domain (MPIIGaze) using low-pass images, respectively. X axis indicates the percentage of high-frequency information filtered out, and the dotted lines illustrate the results when giving original images as input.

To verify this idea, we filter out information of target domain images from high to low-frequency by Fourier transform during testing and see the influence. Particularly, the proportion of information filtered out gradually increases (from 0 to 100%). As shown in Fig. 3, filtering out HFC reduces both the gaze jitter and error, which proves the conjecture that HFC is one of the factors introducing gaze jitter. In addition, the results in Fig. 2(a) also support this conjecture, since HFC is also added when adding random noise. Based on this discovery, reducing the impact of HFC can be an effective direction to improve cross-domain accuracy and reduce gaze jitter.

### 3.3 Domain Adaptation by Contrastive Learning

To reduce the impact of HFC, we propose to utilize contrastive learning. In contrastive learning, positive pairs are generated from a given sample by data augmentations. Then, contrastive loss pulls the features of positive pairs closer. As a result, the model extracts better feature and learns better generalization ability (Kang et al. 2020). The model extracts similar feature from positive pairs and learns to neglect irrelevant differences between positive pairs caused by data augmentation.

Accordingly, we propose to generate such positive pairs from target domain images by adding HFC. Under the con-

strain of contrastive loss, gaze estimation model extracts similar features for positive pairs *i.e.* original image and image with additive HFC. In this way, the impact of HFC are reduced. Consequently, gaze jitter in target domain is reduced and the generalization ability to target domain is improved.

The final question is what type of HFC should be used. In this paper, we show that using adversarial noise to generate positive pairs is effective. First, adversarial noise is a form of HFC (Zhou et al. 2021; Olivier, Raj, and Shah 2021). Second, previous work (Wang et al. 2020) proves that adversarial vulnerability is a indicator when CNN captures HFC. Our experiments show that adversarial noise outperforms other data augmentation methods in Sec. 5.2.

## 4 Method

### 4.1 Overview

First in the data augmentation phase (Sec. 4.2), we use adversarial attacks to add high frequency information to the data and generate positive pairs. Then, the contrastive learning module will reduce the impact of HFC by optimizing the contrastive loss (Sec. 4.3). Finally, we follow the idea of commonly-used adversarial learning to adapt the model to the target domain (Sec. 4.4). An overview of the architecture is described in Fig. 4.

### 4.2 Data Augmentation for Contrastive Learning

**Adversarial Attack** According to Sec. 3.3, adversarial attack is a good choice for data augmentation. Therefore, we use adversarial attacks to add adversarial noise and generate positive pairs. Existing adversarial attacks mainly follow two different ideas, the first one is fast gradient sign method (FGSM)(Goodfellow, Shlens, and Szegedy 2014):

$$x' = x + \epsilon \cdot \text{sign}(\nabla_x \mathcal{L}(f(x), y)), \quad (2)$$

where  $\epsilon$  is the magnitude of the perturbation. This attack is a simple one-step scheme. By contrast, another idea is to use the multi-step variant, which is essentially projected gradient descent (PGD) (Madry et al. 2017a):

$$x^{t+1} = \Pi_{x+S}(x^t + \epsilon \cdot \text{sign}(\nabla_x \mathcal{L}(f(x), y))), \quad (3)$$

where  $\Pi$  is the projection function. In this paper, we simultaneously use FGSM and PGD to generate adversarial noise. Although the noise usually cannot affect human cognition, it can easily fool deep neural networks.

**Adding High-Frequency Component** Here we use adversarial attack described before for data augmentation, where HFC is added to the data. As shown in Fig. 4, our method takes source-target pairs  $(x^s, x^t)$  as inputs. The gaze estimation network  $G(\cdot|\theta_G)$  contains a feature extractor  $F(\cdot|\theta_G)$ , which follows a multi-layer perceptron. Note that the parameters  $\theta_G$  loaded by  $G$  before adaptation are pre-trained with the source domain data  $\mathcal{D}_s$ .

Before adaptation, with the target domain data  $\mathcal{D}_t$  as input, the network  $G(\cdot|\theta_G)$  would generate pseudo labels  $\{y_i^t\}_{i=1}^{N_t}$  by simply forward propagation. At each training

iteration, a batch of  $B$  source-target pairs are randomly sampled from  $\mathcal{D}_s$  and  $\mathcal{D}_t$ , resulting in pairs:  $\{(x_i^s, x_i^t)\}_{i=1}^B$ . Their augmented samples  $\{(x_i^{s,t}, x_i^{t,t})\}_{i=1}^B$  are generated as follow:

$$x_i^{s,t} = \begin{cases} FGSM(x_i^{s,t}, y_i^{s,t}, \mathcal{L}_{gaze}), & 0.5, \\ PGD(x_i^{s,t}, y_i^{s,t}, \mathcal{L}_{gaze}), & 0.5. \end{cases} \quad (4)$$

where  $FGSM$  and  $PGD$  are defined as Eq. (2) and Eq. (3). During adaptation, each image is augmented with 50-50 probability using one of both methods.  $\mathcal{L}_{gaze}$  is usually defined as L1 loss:

$$\mathcal{L}_{gaze}(x, y; \theta_G) = \|G(x|\theta_G) - y\|_1. \quad (5)$$

### 4.3 Contrastive Optimization

As described in Sec. 3.3, we use contrastive learning to reduce the impact of HFC. By encouraging the original and augmented samples to have similar representations, the network learns the ability to learn features with less impact of HFC.

After the data augmentation, we have in total  $4B$  samples  $\{x_i^s, x_i^t, x_i^{s,t}, x_i^{t,t}\}_{i=1}^B$ . Taking a target sample  $x_u^t$  for example, only  $(x_u^t, x_u^{t,t})$  is treated as a positive pair for contrastive learning, the other  $4B - 2$  samples are considered negative ones. Therefore, following the definition from (Chen et al. 2020), we define the contrastive loss  $\ell_{con}(x_u, x_v)$  for a positive pair  $(x_u, x_v)$  as:

$$\ell_{con}(x_u, x_v; \theta_G) = -\log \frac{\exp(\text{sim}(F(x_u|\theta_G), F(x_v|\theta_G))/\tau)}{\sum_{i=1}^{4B} \mathbb{1}_{[i \neq u]} \exp(\text{sim}(F(x_u|\theta_G), F(x_i|\theta_G))/\tau)}, \quad (6)$$

where  $\tau$  is a temperature hyper-parameter (Wu et al. 2018), we empirically set  $\tau = 0.5$ . The similarity measure  $\text{sim}(\mathbf{f}_u, \mathbf{f}_v)$  is defined with dot product as:

$$\text{sim}(\mathbf{f}_u, \mathbf{f}_v) = \frac{\mathbf{f}_u \cdot \mathbf{f}_v}{\|\mathbf{f}_u\| \cdot \|\mathbf{f}_v\|}, \quad (7)$$

In our method, the total contrastive loss  $\mathcal{L}_{con}(x^s, x^t, x^{s,t}, x^{t,t})$  is computed over all positive pairs in a batch.

### 4.4 Adversarial Domain Adaptation

For better adaptation, we follow the idea of commonly-used adversarial learning to adapt the model to new domains. A domain discriminator  $D(\cdot|\theta_D)$  is introduced, and the loss functions are defined as follows to encourage it to play a min-max game with the feature extractor  $F$ .

$$\begin{aligned} \arg \min_{\theta_D} \mathcal{L}_{dis}(x^{s,t}, x^{t,t}; \theta_D) &= -\log(1 - D(F(x^s, x^{s,t})|\theta_D)) \\ &\quad - \log D(F(x^t, x^{t,t})|\theta_D), \\ \arg \min_{\theta_G} \mathcal{L}_{adv}(x^t; \theta_G) &= -\log(1 - D(F(x^t|\theta_G))). \end{aligned} \quad (8)$$

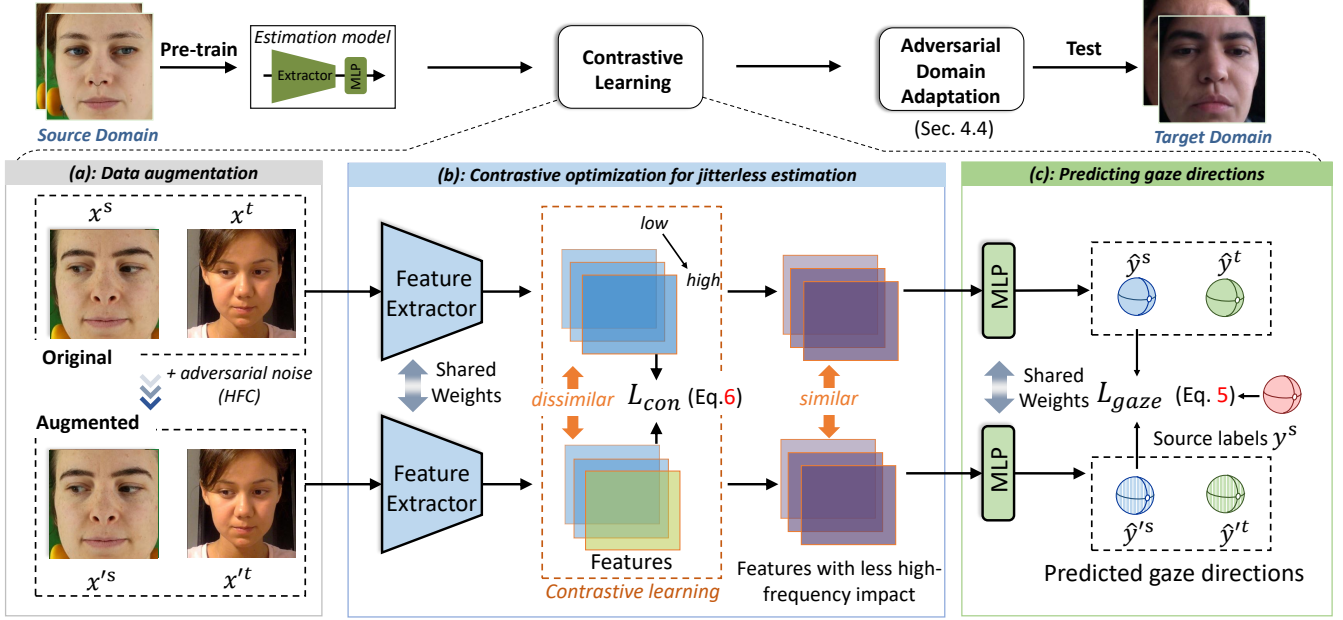


Figure 4: Overview of the proposed framework. (a) At first, pairs of augmented samples are generated by adding HFC with adversarial attack (Sec. 4.2). (b) Contrastive learning encourages the model to learn similar features from the original and adversarial samples, therefore reducing the impact of HFC (Sec. 4.3). (c) Gaze directions are predicted, and the gaze labels from the source domain are employed for constructing the gaze loss.

The adversarial learning follows the classical procedure that are proved to be effective on domain adaptation tasks (Tzeng et al. 2017; Cui et al. 2020). In summary, our goal of optimization on the gaze estimation network is defined as:

$$\begin{aligned} \mathcal{L} = & \mathcal{L}_{gaze}(x^s, y^s; \theta_G) + \mathcal{L}_{gaze}(x'^s, y^s; \theta_G) + \\ & \lambda_1 \mathcal{L}_{con}(x^s, x^t, x'^s, x'^t; \theta_G) + \\ & \lambda_2 (\mathcal{L}_{adv}(x^t; \theta_G) + \mathcal{L}_{adv}(x'^t; \theta_G)), \end{aligned} \quad (9)$$

where  $\lambda_1$  and  $\lambda_2$  are tunable parameters. We empirically set  $\lambda_1 = 1.0$  and  $\lambda_2 = 0.1$  in our experiments.

#### 4.5 Adaptation Procedure

The adaptation procedure is summarized in Algorithm 1. A small amount of data (*i.e.* 100 images) with ground-truth labels from the source domain  $\mathcal{D}_s$  and a small amount of data (*i.e.* 100 images) from the target domain  $\mathcal{D}_t$  are used for unsupervised adaptation. During adaptation, the network  $G(\cdot|\theta_G)$  is trained by minimizing the loss function Eq. (9), and the domain discriminator  $D(\cdot|\theta_D)$  is trained by minimizing the loss function Eq. (8).

## 5 Experiments

### 5.1 Data preparation

Due to the variation in different datasets, data preparation is necessary. In our domain adaptation task, we utilize the ETH-XGaze (E) and Gaze360 (G) dataset as source domains, and MPIIGaze (M) and EyeDiap (D) dataset as target domains.

---

#### Algorithm 1: Our gaze adaptation framework

---

**Input:**  $G(\cdot|\theta_G^{(0)})$  pre-trained on source domain, small  $\mathcal{D}_t$ , and small  $\mathcal{D}_s$ .  
**Output:**  $G(\cdot|\theta_G)$

- 1: **Initialize:**  $y^t \leftarrow G(x^t|\theta_G^{(0)}); D(\cdot|\theta_D^{(0)}) \triangleright \theta_D$  is randomly initialized.
- 2: **for**  $t \leftarrow 1$  **to**  $T$  **do**
- 3:    $(x^s, y^s), x^t \leftarrow \mathcal{D}_s, \mathcal{D}_t$
- 4:    $x'^s, x'^t \leftarrow x^s, y^s, x^t, y^t, G, D$  with Eq. (4)
- 5:    $\mathcal{L}_{gaze} \leftarrow y^s, G(x^s|\theta_G^{(t-1)}), G(x'^s|\theta_G^{(t-1)})$  with Eq. (5)
- 6:    $\mathcal{L}_{adv} \leftarrow x^t, x'^t, G, D$  with Eq. (8)
- 7:    $\mathcal{L}_{con} \leftarrow \frac{1}{4B} \sum_{i=1}^B [\ell_{con}(x_i^t, x_i'^t) + \ell_{con}(x_i'^t, x_i^t) + \ell_{con}(x_i^s, x_i'^s) + \ell_{con}(x_i'^s, x_i^s)]$  with Eq. (6)
- 8:   Update  $G(\cdot|\theta_G^{(t)})$  with Eq. (9)
- 9:    $\mathcal{L}_{dis} \leftarrow x^s, x^t, x'^s, x'^t, G, D$  with Eq. (8)
- 10:   Update  $D(\cdot|\theta_D^{(t)})$  with  $\mathcal{L}_{dis}$
- 11: **end for**

---

The ETH-XGaze dataset (Zhang et al. 2020) provides 80 subjects (*i.e.*, 756,540 images), and we use them all as a source domain. For the Gaze360 dataset (Kellnhofer et al. 2019), we remove the images without subjects' faces and employ the remaining 112,251 images. For the MPIIGaze dataset (Zhang et al. 2017), we adopt the provided evaluation protocol to generate the evaluation set, which contains 3,000

	E→M		E→D		G→M		G→D	
	ma	er	ma	er	ma	er	ma	er
Baseline	3.99	8.56	6.65	8.60	4.38	9.52	6.00	10.05
Low-pass	3.67	7.19	5.85	7.97	5.82	12.33	5.49	17.41
G~0.01	3.07	6.01	5.23	6.63	4.37	8.42	5.44	9.66
G~0.05	3.19	6.46	5.69	6.83	4.56	8.65	5.60	9.17
P~10	3.15	6.48	4.57	6.65	4.57	8.72	5.62	9.28
P~15	3.05	6.25	6.12	7.51	4.56	9.00	5.83	9.57
FGSM	<b>2.09</b>	5.41	5.01	<b>6.62</b>	3.66	7.28	<b>4.41</b>	8.62
PGD	2.19	<b>5.31</b>	5.17	6.83	3.54	7.24	4.58	8.94
Both	2.21	5.35	<b>4.52</b>	<b>6.62</b>	<b>3.51</b>	<b>7.18</b>	<b>4.41</b>	<b>8.61</b>

Table 1: Performance comparison of our method using different image augmentation methods.

images for each subject (*i.e.*, 45,000 images). For the Eye-Diap dataset (Funes Mora, Monay, and Odobez 2014), we employ 16,674 images from 14 subjects under screen target sessions as the evaluation set.

Changes in head poses can significantly affect the appearance of face images. Therefore, we normalized the images following the method in (Zhang et al. 2017), which ensures that the influence of head poses is eliminated.

## 5.2 Ablation Study

**Data Augmentation.** In Sec. 4.2, we combine two adversarial attacks (FGSM and PGD) to add additive HFC to the input images. To prove the optimality, we conduct experiments to compare with other methods to add high-frequency noise. We employ random noises (Gaussian and Poisson) and adversarial noises (FGSM and PGD) to add high-frequency noise respectively. The results are shown in Table 1. We can see that FGSM and PGD each achieve the best results on some tasks, so the final strategy is to use both as augmentation while adaptation (50% probability of each being used), and the results are shown in the "Both" row.

Besides, in Sec. 3.2, directly removing high-frequency can also improve the performance. Therefore, it is also considered one possible data augmentation method in our experiment. So we directly use low-pass data instead of adding HFC during the data augmentation phase, and the results are shown in the "low-pass" row in Table 1. The performance is not as good as adding additive HFC.

**Contrastive Learning.** In this section, we conduct experiments to explore how contrastive loss affects our method's performance. Recall that in Sec. 4.3, we adopt the loss setting from SimCLR (Chen et al. 2020) for implementation. To find the suitable contrastive loss, we further replace this part with the loss settings from the other two commonly-used frameworks MoCo (He et al. 2020) and PCL (Li et al. 2020), respectively.

To this end, we rebuild our method with different contrastive modules, then adapt these modified versions under the same condition. Specifically, for the contrastive loss from MoCo, we utilize a temporal average model to generate the contrastive loss, then we term this version as Ours-MoCo. When it comes to PCL, we follow the settings from

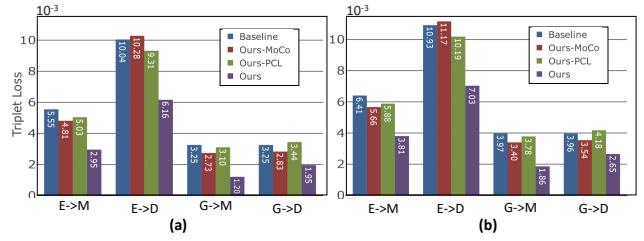


Figure 5: Comparison with other contrastive learning modules on triplet loss with different margins. Lower loss means better reducing the impact of HFC. The margin is set to 0 and  $1 \times 10^{-3}$  in (a) and (b), respectively. Our method is consistently the best.

	E→M		E→D		G→M		G→D	
	ma	er	ma	er	ma	er	ma	er
Baseline	3.99	8.56	6.65	8.60	4.38	9.52	6.00	10.05
Ours-MoCo	3.17	6.48	7.06	9.42	4.79	8.74	5.59	11.60
Ours-PCL	3.25	6.38	6.66	8.52	4.66	8.85	5.35	10.31
Ours	<b>2.21</b>	<b>5.35</b>	<b>4.52</b>	<b>6.62</b>	<b>3.51</b>	<b>7.18</b>	<b>4.41</b>	<b>8.61</b>

Table 2: Performance comparison of our method using different contrastive learning modules.

its original paper and introduce clustering to generate the contrastive loss. This version is named Ours-PCL. For a fair comparison, each of these models uses 100 target samples for UDA, and tests on the whole target domain.

One important indicator of the contrastive learning module is the ability to reduce the impact of HFC. To compare this ability, we use triplet loss (Schroff, Kalenichenko, and Philbin 2015) as an evaluation metric to measure the feature difference between the original and adversarial data. Fig. 5 shows the triplet loss, which reflects the capability of different modules for keeping the consistency before and after being added HFC. In this figure, we find our method gets the consistently lowest triplet loss, even with the variation of margins, which means it better reduces the impact of HFC.

Furthermore, we compare the cross-domain gaze estimation performances with these different contrastive learning modules. Quantitative results are shown in Table 2. Statistical results consistently show that our method also achieves the highest stability and accuracy on these four tasks.

**Ablation.** An ablation study is conducted to demonstrate the effectiveness of each component from our method. The components are shown below.

- CNN: A CNN gaze estimation network using ResNet18 (He et al. 2016). The network is pre-trained on the source domain.
- adv: Adversarial domain adaptation module, which is used to minimize the distance between the source and target domains.
- con: Contrastive learning module, which reduces the impact of HFC by keeping the consistency between original and adversarial samples.

For all the experiments, we load the model trained on the

	E→M		E→D		G→M		G→D	
	<i>mav</i>	<i>error</i>	<i>mav</i>	<i>error</i>	<i>mav</i>	<i>error</i>	<i>mav</i>	<i>error</i>
Baseline	3.99	8.56	6.65	8.60	4.38	9.52	6.00	10.05
CNN+con	2.34	5.37	5.16	6.58	3.79	<b>7.18</b>	4.52	8.62
CNN+adv	3.41	7.24	6.43	7.59	4.11	7.72	5.22	9.86
CNN+con+adv	<b>2.21</b>	<b>5.35</b>	<b>4.52</b>	<b>6.62</b>	<b>3.51</b>	<b>7.18</b>	<b>4.41</b>	<b>8.61</b>

Table 3: Ablation study of different components in our method.

Noise	Model	E→M		G→M	
		<i>mav</i>	<i>error</i>	<i>mav</i>	<i>error</i>
G~0.01	Baseline	4.10	8.79	4.47	9.60
	Ours	<b>2.25</b>	<b>5.36</b>	<b>3.53</b>	<b>7.14</b>
G~0.05	Baseline	6.44	10.61	5.96	10.77
	Ours	<b>4.21</b>	<b>6.37</b>	<b>4.48</b>	<b>6.99</b>
P~10	Baseline	5.76	10.12	5.58	10.50
	Ours	<b>3.56</b>	<b>6.09</b>	<b>4.26</b>	<b>6.99</b>
P~15	Baseline	7.24	11.31	6.47	11.26
	Ours	<b>4.73</b>	<b>6.92</b>	<b>5.04</b>	<b>7.06</b>

Table 4: Comparison of the impact of high-frequency information on the baseline and adapted model. Our method outperforms the baseline, both in values and changes in value.

source domain as initial weights. During adaptation, 100 source samples and 100 target samples are used. Table 3 shows the *mav* and accuracy under different combinations.

It is clear that common adversarial domain adaptation (CNN+adv) has a limited cross-domain performance improvement. After adding the proposed contrastive learning module, our method achieves the best results on all these 4 tasks, which confirms the effectiveness of reducing the impact of HFC.

### 5.3 Resist to High-Frequency Noise

As announced in Sec. 4.3, the contrastive learning module reduces the impact of HFC. To further verify the announcement, we conduct experiments to add high-frequency noise to the test data and compare the impact on the baseline and adapted model brought by the noise.

Specifically, we utilize Gaussian/Poisson noise as additive high-frequency noise and add them to the target data. We take the pre-trained model and adapted models and compare their *mav* and gaze accuracy on the "perturbed" target domain. Quantitative results are shown in Table 4. We find that our method outperforms the baseline, both in comparing their values and their changes in value, which means our method does help the model reduce the impact of HFC.

### 5.4 Performance in Source Domains

In this section, we conduct experiments to verify the performance of the model on the source domain after adaptation to the target domain.

We directly test the model, which has been adapted to the target domain, in the source domain, and the experimental results are shown in Table 5. It can be seen that the *mav* and

	ETH-XGaze		Gaze360	
	<i>mav</i>	<i>error</i>	<i>mav</i>	<i>error</i>
Baseline	<b>0.71</b>	<b>4.42</b>	3.08	<b>11.59</b>
→MPIIGaze	0.75	5.19	<b>2.21</b>	11.86
→EyeDiap	0.77	5.18	2.51	11.98

Table 5: Performance of our method in the source domains after adaptation to the target domains.

	E→M		E→D		G→M		G→D	
	<i>mav</i>	<i>error</i>	<i>mav</i>	<i>error</i>	<i>mav</i>	<i>error</i>	<i>mav</i>	<i>error</i>
Baseline	3.99	8.56	6.65	8.60	4.38	9.52	6.00	10.05
Fine-tune <sup>†</sup>	2.73	4.37	5.35	5.64	3.20	5.63	4.38	5.74
PnP-GA <sup>‡</sup>	2.99	5.53	3.83	5.87	2.76	6.18	5.31	7.92
ADDA*	2.96	7.54	5.11	7.02	3.87	8.16	6.10	11.38
DAGEN*	2.91	5.87	6.56	9.81	4.23	7.70	4.85	12.18
Gaze360	3.28	5.87	6.31	7.38	3.98	7.42	4.89	9.28
GazeAdv	3.66	7.61	6.50	8.27	4.46	8.21	5.63	10.68
GVBGD*	3.00	6.68	5.66	7.27	4.67	8.39	5.23	12.44
PureGaze	3.88	7.08	5.97	7.48	6.16	9.28	5.50	9.32
Ours	<b>2.21</b>	<b>5.35</b>	<b>4.52</b>	<b>6.62</b>	<b>3.51</b>	<b>7.18</b>	<b>4.41</b>	<b>8.61</b>

Table 6: Comparison with state-of-the-art unsupervised domain adaptation approaches. <sup>†</sup> indicates that target gaze labels are used. <sup>‡</sup> indicates that experimental settings are different. \* indicates that more than 100 target samples are used during adaptation.

gaze error of the adapted model increase only slightly, and the *mav* even decreases on the Gaze360 dataset. This indicates that our method can also continue to maintain its performance in source domains after adaptation.

### 5.5 Comparison with SOTA UDA Methods

We also compare the UDA performances between our method and other state-of-the-art UDA methods.

DAGEN (Guo et al. 2020), GazeAdv (Wang et al. 2019), Gaze360 (Kellnhofer et al. 2019), PnP-GA (Liu et al. 2021c), and PureGaze (Cheng, Bao, and Lu 2022) propose different methods for cross-domain gaze estimation. It is worth noting that PnP-GA requires a specific group of models (10 models) for effective domain adaptation, so the method is under different settings from others. In contrast, the ADDA (Tzeng et al. 2017) and GVBGD (Cui et al. 2020) were originally proposed for classification tasks. Here, we conduct experiments with these two methods to show the performance of state-of-the-art UDA methods on cross-domain gaze estimation. All the backbones are replaced with ResNet18, which is the same as ours for a fair comparison. In detail, we also adjust the number of samples to reach the best performance of these methods.

Quantitative results are shown in Table 6. The results of fine-tuning are shown as the upper bound of adaptation, it uses 100 samples which is the same as ours. We found that our method significantly outperforms the state-of-the-art UDA methods. The superior performance of our method validates the effectiveness of our method for cross-domain gaze estimation.

## 6 Conclusion

In this paper, we present a novel framework for adapting gaze estimation to new domains. We start by analyzing the gaze jitter phenomenon that occurs when crossing domains, and discover that HFC is one important factor leading to gaze jitter. This factor guides us to design the proposed method. Extensive experiments demonstrate the superior performance of our method for cross-domain gaze estimation tasks. Our method has the potential to be used in real-world gaze estimation applications.

## References

- Admoni, H.; and Scassellati, B. 2017. Social eye gaze in human-robot interaction: a review. *Journal of Human-Robot Interaction*, 6(1): 25–63.
- Bousmalis, K.; Trigeorgis, G.; Silberman, N.; Krishnan, D.; and Erhan, D. 2016. Domain separation networks. *Advances in neural information processing systems*, 29: 343–351.
- Cai, M.; Lu, F.; and Sato, Y. 2020. Generalizing hand segmentation in egocentric videos with uncertainty-guided model adaptation. In *Proceedings of the IEEE/CVF Conference on Computer Vision and Pattern Recognition*, 14392–14401.
- Chen, T.; Kornblith, S.; Norouzi, M.; and Hinton, G. 2020. A simple framework for contrastive learning of visual representations. In *International conference on machine learning*, 1597–1607. PMLR.
- Cheng, Y.; Bao, Y.; and Lu, F. 2022. Puregaze: Purifying gaze feature for generalizable gaze estimation. In *Proceedings of the AAAI Conference on Artificial Intelligence*, volume 36, 436–443.
- Cheng, Y.; Huang, S.; Wang, F.; Qian, C.; and Lu, F. 2020. A coarse-to-fine adaptive network for appearance-based gaze estimation. In *Proceedings of the AAAI Conference on Artificial Intelligence*, volume 34, 10623–10630.
- Cui, S.; Wang, S.; Zhuo, J.; Su, C.; Huang, Q.; and Tian, Q. 2020. Gradually vanishing bridge for adversarial domain adaptation. In *Proceedings of the IEEE/CVF Conference on Computer Vision and Pattern Recognition*, 12455–12464.
- Demiris, Y. 2007. Prediction of intent in robotics and multi-agent systems. *Cognitive processing*, 8(3): 151–158.
- Funes Mora, K. A.; Monay, F.; and Odobez, J.-M. 2014. Eyediap: A database for the development and evaluation of gaze estimation algorithms from rgb and rgb-d cameras. In *Proceedings of the Symposium on Eye Tracking Research and Applications*, 255–258.
- Ganin, Y.; and Lempitsky, V. 2015. Unsupervised domain adaptation by backpropagation. In *International conference on machine learning*, 1180–1189. PMLR.
- Ghifary, M.; Kleijn, W. B.; and Zhang, M. 2014. Domain adaptive neural networks for object recognition. In *Pacific Rim international conference on artificial intelligence*, 898–904. Springer.
- Glorot, X.; Bordes, A.; and Bengio, Y. 2011. Domain adaptation for large-scale sentiment classification: A deep learning approach. In *ICML*.
- Goodfellow, I.; Pouget-Abadie, J.; Mirza, M.; Xu, B.; Warde-Farley, D.; Ozair, S.; Courville, A.; and Bengio, Y. 2014. Generative adversarial nets. *Advances in neural information processing systems*, 27.
- Goodfellow, I. J.; Shlens, J.; and Szegedy, C. 2014. Explaining and harnessing adversarial examples. *arXiv preprint arXiv:1412.6572*.
- Guo, Z.; Yuan, Z.; Zhang, C.; Chi, W.; Ling, Y.; and Zhang, S. 2020. Domain adaptation gaze estimation by embedding with prediction consistency. In *Proceedings of the Asian Conference on Computer Vision*.
- He, K.; Fan, H.; Wu, Y.; Xie, S.; and Girshick, R. 2020. Momentum contrast for unsupervised visual representation learning. In *Proceedings of the IEEE/CVF Conference on Computer Vision and Pattern Recognition*, 9729–9738.
- He, K.; Zhang, X.; Ren, S.; and Sun, J. 2016. Deep residual learning for image recognition. In *Proceedings of the IEEE conference on computer vision and pattern recognition*, 770–778.
- Kang, G.; Jiang, L.; Wei, Y.; Yang, Y.; and Hauptmann, A. G. 2020. Contrastive adaptation network for single-and multi-source domain adaptation. *IEEE transactions on pattern analysis and machine intelligence*.
- Kellnhofer, P.; Recasens, A.; Stent, S.; Matusik, W.; and Torralba, A. 2019. Gaze360: Physically unconstrained gaze estimation in the wild. In *Proceedings of the IEEE/CVF International Conference on Computer Vision*, 6912–6921.
- Li, J.; Zhou, P.; Xiong, C.; and Hoi, S. C. 2020. Prototypical contrastive learning of unsupervised representations. *arXiv preprint arXiv:2005.04966*.
- Liu, A.; Liu, X.; Yu, H.; Zhang, C.; Liu, Q.; and Tao, D. 2021a. Training robust deep neural networks via adversarial noise propagation. *IEEE Transactions on Image Processing*, 30: 5769–5781.
- Liu, W.; Ferstl, D.; Schuster, S.; Zebedin, L.; Fua, P.; and Leistner, C. 2021b. Domain adaptation for semantic segmentation via patch-wise contrastive learning. *arXiv preprint arXiv:2104.11056*.
- Liu, Y.; Liu, R.; Wang, H.; and Lu, F. 2021c. Generalizing Gaze Estimation with Outlier-guided Collaborative Adaptation. In *Proceedings of the IEEE/CVF International Conference on Computer Vision*, 3835–3844.
- Lu, F.; Sugano, Y.; Okabe, T.; and Sato, Y. 2014. Adaptive linear regression for appearance-based gaze estimation. *IEEE transactions on pattern analysis and machine intelligence*, 36(10): 2033–2046.
- Ma, X.; Niu, Y.; Gu, L.; Wang, Y.; Zhao, Y.; Bailey, J.; and Lu, F. 2021. Understanding adversarial attacks on deep learning based medical image analysis systems. *Pattern Recognition*, 110: 107332.
- Madry, A.; Makelov, A.; Schmidt, L.; Tsipras, D.; and Vladu, A. 2017a. Towards deep learning models resistant to adversarial attacks. *arXiv preprint arXiv:1706.06083*.
- Madry, A.; Makelov, A.; Schmidt, L.; Tsipras, D.; and Vladu, A. 2017b. Towards deep learning models resistant to adversarial attacks. *arXiv preprint arXiv:1706.06083*.

- Majoranta, P.; and Bulling, A. 2014. Eye tracking and eye-based human-computer interaction. In *Advances in physiological computing*, 39–65. Springer.
- Moosavi-Dezfooli, S.-M.; Fawzi, A.; and Frossard, P. 2016. Deepfool: a simple and accurate method to fool deep neural networks. In *Proceedings of the IEEE conference on computer vision and pattern recognition*, 2574–2582.
- Olivier, R.; Raj, B.; and Shah, M. 2021. High-frequency adversarial defense for speech and audio. In *ICASSP 2021-2021 IEEE International Conference on Acoustics, Speech and Signal Processing (ICASSP)*, 2995–2999. IEEE.
- Park, H. S.; Jain, E.; and Sheikh, Y. 2013. Predicting primary gaze behavior using social saliency fields. In *Proceedings of the IEEE International Conference on Computer Vision*, 3503–3510.
- Park, S.; Mello, S. D.; Molchanov, P.; Iqbal, U.; Hilliges, O.; and Kautz, J. 2019. Few-shot adaptive gaze estimation. In *Proceedings of the IEEE/CVF International Conference on Computer Vision*, 9368–9377.
- Schroff, F.; Kalenichenko, D.; and Philbin, J. 2015. Facenet: A unified embedding for face recognition and clustering. In *Proceedings of the IEEE conference on computer vision and pattern recognition*, 815–823.
- Shrivastava, A.; Pfister, T.; Tuzel, O.; Susskind, J.; Wang, W.; and Webb, R. 2017. Learning from simulated and unsupervised images through adversarial training. In *Proceedings of the IEEE conference on computer vision and pattern recognition*, 2107–2116.
- Su, J.; Vargas, D. V.; and Sakurai, K. 2019. One pixel attack for fooling deep neural networks. *IEEE Transactions on Evolutionary Computation*, 23(5): 828–841.
- Szegedy, C.; Zaremba, W.; Sutskever, I.; Bruna, J.; Erhan, D.; Goodfellow, I.; and Fergus, R. 2013. Intriguing properties of neural networks. *arXiv preprint arXiv:1312.6199*.
- Terzioğlu, Y.; Mutlu, B.; and Şahin, E. 2020. Designing social cues for collaborative robots: the role of gaze and breathing in human-robot collaboration. In *Proceedings of the 2020 ACM/IEEE International Conference on Human-Robot Interaction*, 343–357.
- Tzeng, E.; Hoffman, J.; Saenko, K.; and Darrell, T. 2017. Adversarial discriminative domain adaptation. In *Proceedings of the IEEE conference on computer vision and pattern recognition*, 7167–7176.
- Wang, H.; Dong, X.; Chen, Z.; and Shi, B. E. 2015. Hybrid gaze/EEG brain computer interface for robot arm control on a pick and place task. In *2015 37th Annual International Conference of the IEEE Engineering in Medicine and Biology Society (EMBC)*, 1476–1479. IEEE.
- Wang, H.; Wu, X.; Huang, Z.; and Xing, E. P. 2020. High-frequency component helps explain the generalization of convolutional neural networks. In *Proceedings of the IEEE/CVF Conference on Computer Vision and Pattern Recognition*, 8684–8694.
- Wang, K.; Zhao, R.; Su, H.; and Ji, Q. 2019. Generalizing eye tracking with bayesian adversarial learning. In *Proceedings of the IEEE/CVF Conference on Computer Vision and Pattern Recognition*, 11907–11916.
- Wang, M.; and Deng, W. 2018. Deep visual domain adaptation: A survey. *Neurocomputing*, 312: 135–153.
- Wang, Z.; Bovik, A. C.; Sheikh, H. R.; and Simoncelli, E. P. 2004. Image quality assessment: from error visibility to structural similarity. *IEEE transactions on image processing*, 13(4): 600–612.
- Wu, Z.; Xiong, Y.; Yu, S. X.; and Lin, D. 2018. Unsupervised feature learning via non-parametric instance discrimination. In *Proceedings of the IEEE conference on computer vision and pattern recognition*, 3733–3742.
- Yang, J.; Li, C.; An, W.; Ma, H.; Guo, Y.; Rong, Y.; Zhao, P.; and Huang, J. 2021. Exploring Robustness of Unsupervised Domain Adaptation in Semantic Segmentation. *arXiv preprint arXiv:2105.10843*.
- Yu, C.; Wang, J.; Chen, Y.; and Huang, M. 2019. Transfer learning with dynamic adversarial adaptation network. In *2019 IEEE International Conference on Data Mining (ICDM)*, 778–786. IEEE.
- Yu, Y.; Liu, G.; and Odobez, J.-M. 2019. Improving few-shot user-specific gaze adaptation via gaze redirection synthesis. In *Proceedings of the IEEE/CVF Conference on Computer Vision and Pattern Recognition*, 11937–11946.
- Zhang, X.; Park, S.; Beeler, T.; Bradley, D.; Tang, S.; and Hilliges, O. 2020. ETH-XGaze: A large scale dataset for gaze estimation under extreme head pose and gaze variation. In *European Conference on Computer Vision*, 365–381. Springer.
- Zhang, X.; Sugano, Y.; Fritz, M.; and Bulling, A. 2017. Mpi-gaze: Real-world dataset and deep appearance-based gaze estimation. *IEEE transactions on pattern analysis and machine intelligence*, 41(1): 162–175.
- Zhou, Y.; Hu, X.; Han, J.; Wang, L.; and Duan, S. 2021. High frequency patterns play a key role in the generation of adversarial examples. *Neurocomputing*, 459: 131–141.
- Zhu, Y.; Zhuang, F.; Wang, J.; Ke, G.; Chen, J.; Bian, J.; Xiong, H.; and He, Q. 2020. Deep subdomain adaptation network for image classification. *IEEE transactions on neural networks and learning systems*, 32(4): 1713–1722.